Vibration Suppression for Active Magnetic Bearings Using Adaptive Filter with Iterative Search Algorithm

Jin-Hui Ye, *Student Member*, *IEEE*, Dan Shi, *Member*, *IEEE*, Yue-Sheng Qi, *Student Member*, *IEEE*, Jin-Hui Gao, *Student Member*, *IEEE*, and Jian-Xin Shen, *Senior Member*, *CES*, and *IEEE*

***Abstract*—Active Magnetic Bearing (AMB) is a kind of electromagnetic support that makes the rotor movement frictionless and can suppress rotor vibration by controlling the magnetic force. The most common approach to restrain the rotor vibration in AMBs is to adopt a notch filter or adaptive filter in the AMB controller. However, these methods cannot obtain the precise amplitude and phase of the compensation current. Thus, they are not so effective in terms of suppressing the vibrations of the fundamental and other harmonic orders over the whole speed range. To improve the vibration suppression performance of AMBs, an adaptive filter based on Least Mean Square (LMS) is applied to extract the vibration signals from the rotor displacement signal. An Iterative Search Algorithm (ISA) is proposed in this paper to obtain the corresponding relationship between the compensation current and vibration signals. The ISA is responsible for searching the compensating amplitude and shifting phase online for the LMS filter, enabling the AMB controller to generate the corresponding compensation force for vibration suppression. The results of ISA are recorded to suppress vibration using the Look-Up Table (LUT) in variable speed range. Comprehensive simulations and experimental validations are carried out in fixed and variable speed range, and the results demonstrate that by employing the ISA, vibrations of the fundamental and other harmonic orders are suppressed effectively.**

***Index Terms*—Active Magnetic Bearing (AMB), Adaptive filter, Iterative search algorithm, Least mean square (LMS), Vibration suppression.**

I. Introduction

ACTIVE Magnetic Bearing (AMB) is a kind of support system that levitates the rotor by electromagnetic force. With the development of industry, AMB has been applied in more and more applications due to its excellent properties such as no need for lubrication, low maintenance cost, and long lifespan [1].

An important factor to consider in the operation of AMB is the vibration, as it can serve as a severe problem. The vibration can cause collision of the rotor and the backup bearings, resulting in damaging the AMB. Similarly, the vibration signals of rotor displacement feedback can disturb the controller and cause current oscillation, which ultimately affects the stability of the AMB system. Various researches have been carried out to solve AMB's vibration problem, and generally these methods can be classified into two categories: automatic balancing and vibration suppression [2]. The goal of automatic balancing is to make the rotor rotate around the inertial axis, and vibration suppression forces the rotor to rotate around the geometric axis.

By applying automatic balancing methods, the vibration signals do not cause current oscillation in AMB's coils and hence cannot be transmitted to AMB's stator or housing. The notch filter is usually used as the feedforward input of the AMB controller to achieve automatic balancing [3]-[5]. However, the notch filter might make the AMB system unstable, and it needs to be compensated [6]-[7]. Methods such as adaptive auto-centering control [8], automatic learning control [9], and robust fuzzy control [10] have been applied in automatic balancing. These methods can effectively restrain the current oscillation. In practice, AMB's rotor might contain current oscillations of multi-frequencies, and the most common method is applying multiple notch filters to the AMB controller [11]-[14].

From the 1980s, research on vibration suppression of the AMB has been carried out. The notch filter is applied and behaves effectively under constant speed operation [3], [15]. The adaptive filter based on Least Mean Square (LMS) is widely used in AMB vibration suppression due to its excellent performance and easy implementation [16]-[19]. However, a notch filter or adaptive filter could not always make the AMB system stable in a wide speed range. Various improvements to the notch filter and adaptive filter have been proposed to extend the applicability. Shi et al. adjusted the LMS step through fuzzy control to stabilize the system [20]. Peng et al. proposed a two-stage notch filter to

Manuscript received October, 25, 2023; revised January 14, 2024; accepted February 19, 2024. Date of publication March 25, 2024. Date of current version February 21, 2024.

This work was supported by the Natural Science Foundation of China (U22A20214). (*Corresponding Authors*: *Dan Shi and Jian-Xin Shen*)

Jin-Hui Ye, Dan Shi, Yue-Sheng Qi, Jin-Hui Gao, and Jian-Xin Shen are with Department of Electrical Engineering, Zhejiang University, Hangzhou 310027, China (e-mail: 22110150@zju.edu.cn, shidan_ee@zju.edu.cn, 3190104924@zju.edu.cn, 22110047@zju.edu.cn, J_X_Shen@ zju.edu.cn).

Digital Object Identifier 10.30941/CESTEMS.2024.00007

eliminate the influence of the gyroscopic effect on the notch filter [21]. Sun et al. applied a generalized integrator and frequency locked loop to realize vibration suppression without angular sensors [22].

A further improvement method is to compensate for the phase and amplitude of the filter's output. Peng *et al.* proposed the phase lead compensation to adjust the phase of the notch filter's output [6]. Gong *et al.* proposed the polarity switching notch filter and determined the notch filter's polarity by the root locus of the system [23]-[24]. By compensating for the phase or amplitude of the notch filter, the above methods can make AMB stable in the whole speed range. However, when the phase or polarity is switched, severe oscillation will occur [23]. Besides, precise parameters of AMB are required in the above methods for calculation, and deviation of the parameters from AMB's actual values makes these methods unsuitable for manufacture.

Various online search methods have been proposed to automatically compensate for the phase and amplitude of adaptive filters and maintain stability in the whole operational speed range of AMB systems. Jiang *et al.* introduced a recursive seeking method that searches compensation phase and amplitude in the Cartesian coordinate system [25]. This method is referred to as the Fixed Angle Compensate (FAC) because it operates with a fixed searching angle. In consideration of the limited flexibility of FAC due to its fixed searching angle, Gong et al. introduced the Variable Angle Compensation (VAC) [26]-[27]. VAC employs a variable searching angle to enhance its speed and accuracy. However, its angle iterative formula is sensitive to parameters, and improper parameter settings or initial angle might lead to system failure. On the basis of FAC and VAC, this paper introduces the Iterative Search Algorithm (ISA) to compensate for the LMS adaptive filter. The Adaptive Filter with Compensation (AFC) is developed by combining the ISA and LMS adaptive filter, which can generate a compensation force in the AMB to suppress the rotor vibration.

This paper is arranged as follows. In section II, the mathematical model of the AMB system is established, with the consideration of both one degree of freedom (1-DOF) and five degrees of freedom (5-DOFs). Section III explains the principle of vibration suppression strategy, including LMS adaptive filter and the ISA. In section IV, the simulation results of AFC are presented. In section V, the 1st-3rd order AFCs are applied to an AMB system with a rigid rotor, and experimental results are presented to validate AFC's effectiveness in the whole speed range. In section VI, the conclusion of this paper is summarized.

II. MODELING

A. Modeling of 1-DOF AMB Rigid Rotor System

An AMB system mainly consists of a rotor, a controller, electromagnets, and sensors. The diagram of the 1-DOF AMB system is shown in Fig. 1. A displacement-current close loop control architecture is adopted in the AMB system. The outer loop is a displacement loop, making the AMB system a stable closed-loop system. The inner loop is a current loop, improving AMB's current response greatly. The 1-DOF AMB system is modeled as follows.

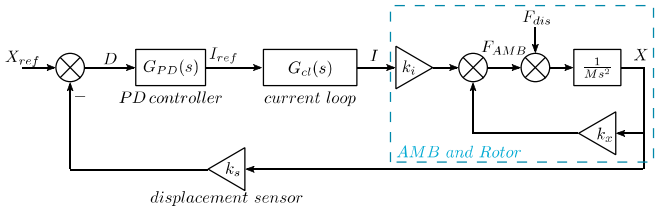

Fig. 1. Diagram of 1-DOF AMB system.

According to Newton's law of motion, the dynamic differential equation of the rotor is expressed as:

$$F_{\text{AMB}} + F_{\text{dis}} = M\ddot{x} \tag{1}$$

where F_{AMB} is the electromagnetic force output by AMB, F_{dis} is the source of disturbances, M is the rotor's mass, and x is the rotor's displacement. The linear expression of F_{AMB} is given by [28]:

$$F_{\text{AMB}} = k_i I + k_x x \tag{2}$$

where k_i and k_x are the force-current stiffness and force-displacement stiffness, both of which are intrinsic parameters of AMB, and I is the control current in AMB's coils. Ignoring F_{dis}, the transfer function of the AMB and the rigid rotor is obtained by combining (1) and (2) in the frequency domain:

$$G_{\text{AMB}}(s) = \frac{X(s)}{I(s)} = \frac{k_i}{Ms^2 - k_x} \tag{3}$$

where s is the Laplace Operator. As $k_x > 0$, one of AMB's open loop poles is in the right half of the complex plane. Thus the AMB system is unstable, and a closed-loop controller is needed.

The displacement sensor is often regarded as a first order inertial element, as the cut-off frequency of the displacement sensor is usually far higher than the frequency of the rotor vibration. The displacement sensor can be modeled as a gain k_s. The controller's input D is obtained by comparing the rotor displacement reference $X_{\text{ref}}(s)$ with the $X(s)$. Since the goal of AMB is to levitate the rotor at the center of the air gap, $X_{\text{ref}}(s)$ is generally set to 0, then:

$$D(s) = -k_s X(s) \tag{4}$$

The Proportional-integral-ferivative (PID) control is widely used in the field of AMB control. The function of the proportional coefficient K_P is to adjust the AMB's stiffness. The differential coefficient K_D is used to adjust AMB's damping. The integral coefficient K_I is used to eliminate steady-state errors. But it has little effect in theoretical analysis; hereafter, it is omitted. Thus a PD controller is adopted for the displacement loop, and the corresponding transfer function is expressed as:

$$G_{PD}(s) = K_P + K_D s \tag{5}$$

The current loop consists of the PI controller, amplifier, AMB's coil and current sensor, and its diagram is shown in Fig. 2.

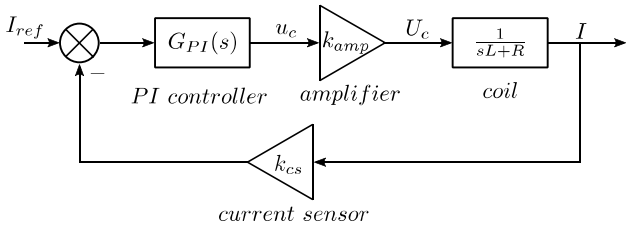

Fig. 2. Diagram of current loop.

The current sensor and power amplifier have low-pass characteristics, and they are regarded as first-order inertial elements. In this paper, their cut-off frequencies are much higher than the rotor vibration's frequency. Hence they are considered as gain segments k_{cs} and k_{amp}. The AMB coil can be modeled as a resistor and an inductor connected in series:

$$G_{\text{coil}}(s)=\frac{1}{sL+R} \tag{6}$$

where L is the coil's induction, and R is the coil's resistance. The time constant $\tau=\frac{L}{R}$ is very large, and affects the current's response speed significantly. Therefore, the PI parameters are adjusted by pole-zero cancellation to optimize the response of the current loop, and the transfer function of the current loop is derived:

$$G_{cl}(s)=\frac{I}{I_{\text{ref}}}=\frac{1}{k_{cs}(\frac{s}{f_c}+1)} \tag{7}$$

where I_{ref} is the control current reference, f_c is the cut-off frequency of $G_{cl}(s)$. By setting f_c much higher than the frequency of rotor vibration, $G_{cl}(s)$ can be simplified as a gain segment:

$$G_{cl}(s)=\frac{1}{k_{cs}} \tag{8}$$

By combining (2)-(8), F_{AMB} generated by the close loop AMB system can be expressed as:

$$F_{\text{AMB}}(s)=-(K_{\text{AMB}}+sD_{\text{AMB}})X(s) \tag{9}$$

where K_{AMB} and D_{AMB} are stiffness and damping of the close loop AMB system respectively, and they are expressed as:

$$\begin{cases} K_{\text{AMB}}=\dfrac{k_s k_i}{k_{cs}}K_P-k_x \\ D_{\text{AMB}}=\dfrac{k_s k_i}{k_{cs}}K_D \end{cases} \tag{10}$$

The system stiffness and damping have a considerable impact on the stability and performance of the AMB system, and Schweitzer et al. proposed "natural stiffness" and "natural damping" [2] as a basis for setting the proper value of them:

$$\begin{cases} K_{\text{AMB}}\in[k_x,10k_x] \\ D_{\text{AMB}}\in(0,2\sqrt{MK_{\text{AMB}}}) \end{cases} \tag{11}$$

On the basis of equation (11) and through means of trial and error, the following parameters show excellent performance for the AMB system investigated in this paper:

$$\begin{cases} K_{\text{AMB}}=4k_x \\ D_{\text{AMB}}=\sqrt{MK_{\text{AMB}}} \end{cases} \tag{12}$$

According to (1)-(12), the transfer function for the AMB system with input $F_{\text{dis}}(s)$ and output $X(s)$ is expressed as:

$$G_{\text{XF}}(s)=\frac{X(s)}{F_{\text{dis}}(s)}=\frac{1}{Ms^2+2\sqrt{Mk_x}s+4k_x} \tag{13}$$

During AMB operation, disturbances such as rotor unbalance and displacement sensor runout [13], might produce vibration whose frequency is the rotating speed ω_r or k (assuming that $k=1$ to n) times that of ω_r. Thus in the whole speed range, disturbances' frequencies might be between $\omega_{r[\min]}$ and $n\omega_{r[\max]}$. To simplify, replace $[\omega_{r[\min]},n\omega_{r[\max]}]$ with $[\omega_1,\omega_2]$.

The bode plot of $G_{\text{XF}}(s)$ is shown in Fig. 3, which shows that $G_{\text{XF}}(s)$ has a large gain in $[\omega_1,\omega_2]$. That is to say, these disturbances will cause severe vibration within the range of $[\omega_1,\omega_2]$. Moreover, the phase of $G_{\text{XF}}(s)$ is changeable in $[\omega_1,\omega_2]$, which means that the vibration suppression strategy should be able to compensate for the phase effectively.

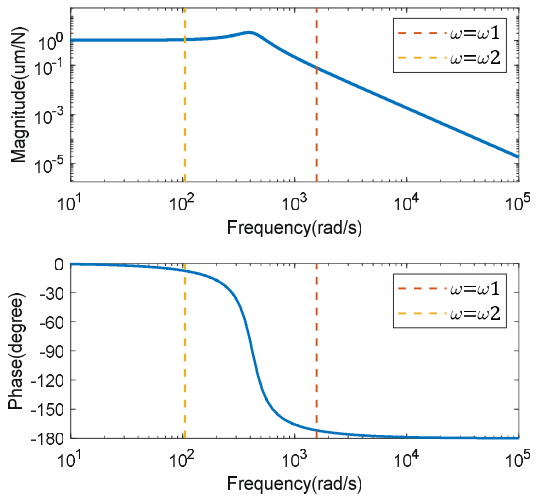

Fig. 3. Bode plot of $G_{\text{XF}}(s)$.

B. Structure of 5-DOFs AMB Controller

In AMB and rigid rotor system, the motion of the rotor can be divided into 6 degrees of freedom (DOFs), which includes displacement along the *x*, *y* and *z*-axis as (*x*, *y*, *z*), rotation around the *x*, *y* and *z*-axis as $(\theta_x,\theta_y,\theta_z)$. The motor controls θ_z while $[x,y,\theta_x,\theta_y,z]$ are controlled by AMB. In this paper, $[x_1,x_2,y_1,y_2,z]$ are used to represent the motion in 5-DOFs, which can be obtained from $[x,y,\theta_x,\theta_y,z]$ through a linear transformation. A general AMB system is combined with two radial magnetic bearings (RMBs) and one thrust magnetic

bearing (TMB). The dynamic equation of 5-DOFs AMB and rigid rotor system is expressed as:

$$\begin{cases} M\ddot{x} = F_{x1} + F_{x2} + F_{x\text{dis}} \\ M\ddot{y} = F_{y1} + F_{y2} + F_{y\text{dis}} \\ M\ddot{z} = F_{z} + F_{z\text{dis}} \\ \ddot{\theta}_x + \dfrac{\omega_r J_z}{J_{xy}}\dot{\theta}_y = -\dfrac{l_1}{J_{xy}}F_{y1} + \dfrac{l_2}{J_{xy}}F_{y2} + \dfrac{1}{J_{xy}}M_{x\text{dis}} \\ \ddot{\theta}_y - \dfrac{\omega_r J_z}{J_{xy}}\dot{\theta}_x = \dfrac{l_1}{J_{xy}}F_{x1} - \dfrac{l_2}{J_{xy}}F_{x2} + \dfrac{1}{J_{xy}}M_{y\text{dis}} \end{cases} \tag{14}$$

where $\left[F_{x1}, F_{x2}, F_{y1}, F_{y2}, F_z\right]$ represent the electromagnetic force of the RMBs and TMB on the rotor respectively, $\left[F_{x\text{dis}}, F_{y\text{dis}}, F_{z\text{dis}}, M_{x\text{dis}}, M_{y\text{dis}}\right]$ represent the component of the disturbance in 5 DOFs, J_{xy} and J_z are the moment of inertia of the rotor in the radial and axial directions, l_1 and l_2 are the axial displacements of rotor's geometric center to RMBs, and ω_r is the rotating speed along z-axis.

Fig. 4 shows a decentralized control system widely used in industrial AMB system with rigid rotor. Practice has proved that it works well and has acceptable performance [2]. Due to its simple structure and great robustness, decentralized control is adopted for the 5-DOFs AMB system investigated in this paper.

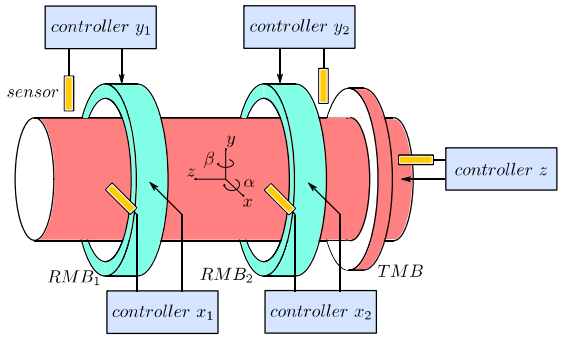

Fig. 4. Diagram of 5-DOFs AMB control system.

III. Principle of Vibration Suppress Strategy

A. Adaptive Filter Based on LMS

LMS is an adaptive algorithm based on the principle of gradient descent. Due to its low complexity and excellent performance, it has been widely used in AMB. The schematic diagram of LMS is shown in Fig. 5, and the implementation of LMS can be expressed as:

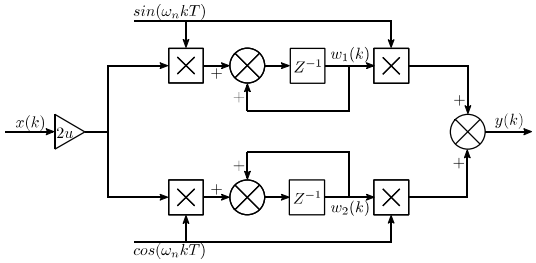

Fig. 5. Diagram of basic LMS.

$$\begin{cases} y(k) = w_1(k)\sin(\omega_n kT) + w_2(k)\cos(\omega_n kT) \\ w_1(k+1) = w_1(k) + 2ux(k)\sin(\omega_n kT) \\ w_2(k+1) = w_2(k) + 2ux(k)\cos(\omega_n kT) \end{cases} \tag{15}$$

where k is the argument of LMS, $x(k)$, $y(k)$ is LMS's input and output respectively, T is the sampling period, u is the step size, ω_n is the notch frequency of LMS, and $w_1(k)$, $w_2(k)$ is the weight coefficients of the sine and cosine components of $y(k)$.

The transfer function of the LMS $G_{LMS}(z)$ is derived as:

$$G_{\text{LMS}}(z) = \frac{2u(z\cos(\omega_n T) - 1)}{z^2 - 2z\cos(\omega_n T) + 1} \tag{16}$$

The pole of $G_{\text{LMS}}(z)$ is $z = exp(j\omega_n T)$, and gain of $G_{\text{LMS}}(z)$ is infinite at its pole. Henceforth, by using $G_{\text{LMS}}(z)$ to construct a close loop system, an adaptive filter is obtained. The transfer function of the LMS adaptive filter is:

$$G_{\text{AF}}(z) = \frac{2u(z\cos(\omega_n T) - 1)}{z^2 + 2z(u-1)\cos(\omega_n T) + 1 - 2u} \tag{17}$$

The bode plot of G_{AF} is shown in Fig. 6. The gain of G_{AF} is nearly 1 and the phase lag is nearly 0 when $\omega = \omega_n$. And the gain is close to 0 when $\omega \neq \omega_n$. Thus G_{AF} can extract the vibration signal whose frequency is ω_n. It is worth mentioning that the frequencies of vibrations in AMB are usually ω_r or an integral multiple of ω_r. For example, by setting $\omega_n = \omega_r$, the LMS adaptive filter can extract the fundamental vibration signal from the rotor displacement signal.

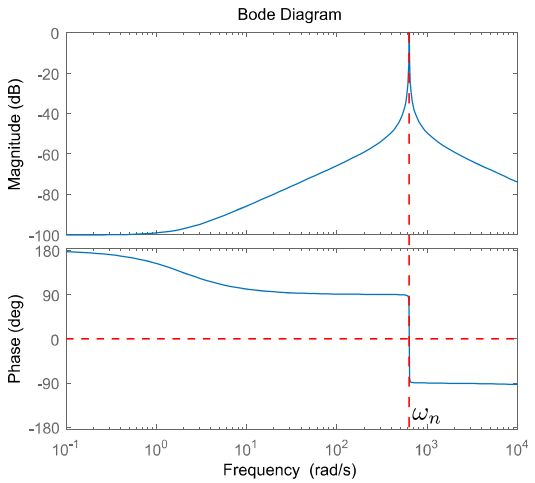

Fig. 6. Bode plot of G_{AF}.

B. Adaptive Filter with Compensation Based on Iterative Search Algorithm

The LMS adaptive filter can extract vibration signal with a certain frequency from the rotor displacement signal. In the vibration suppression of AMB, it is necessary to generate a resisting force F_{AMB} to restrain the disturbances. According to

(2), the AMB controller should generate a compensation current I_{comp} having the same frequency as F_{dis}.

To obtain the I_{comp}, the LMS adaptive filter is applied to extract vibration signal whose frequency is ω_r. Then with proper amplitude and phase compensation to the LMS's output $Y(s)$, I_{comp} is obtained:

$$I_{\text{comp}} = AY(s)e^{-\frac{\phi}{\omega_r}} \tag{18}$$

where A is compensation amplitude, ϕ is phase shifting angle. Assuming that there is only rotational frequency vibration caused by rotor unbalance, simulation model is built and compensation current with different $[A,\phi]$ is applied to the LMS. The result is shown in Fig. 7, and it illustrates that there is an optimal $[A,\phi]$ for vibration suppression.

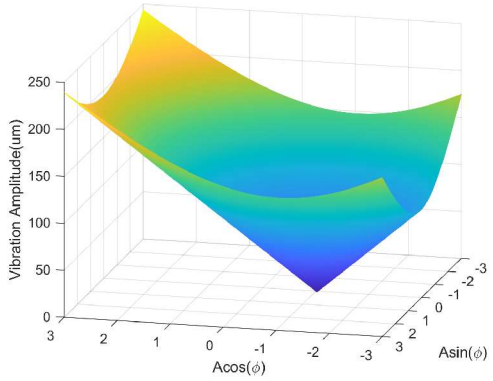

Fig. 7. Rotor vibration affected by $[A,\phi]$.

But in practice, the relationship between rotor vibration and $[A,\phi]$ cannot be built precisely due to the parameter uncertainties and unknown nonlinear disturbances. Therefore, an ISA is proposed, which compensates the output of the adaptive filter through $[A,\phi]$. The ISA searches $[A,\phi]$ iteratively through the rotor vibration amplitude V_{in}, making V_{in} smaller.

However it is still difficult to establish a corresponding relationship between a single input (V_{in}) and two outputs (A,ϕ). The ISA start with the initial values $[A_0,\phi_0]$. It can be seen from Fig. 7 that the improper initial values will increase rotor vibration and reduce the convergence speed of ISA. In this paper, $[A_0,\phi_0]$ are set to $[0,0]$, which keeps the rotor vibration the same as without the ISA. The ISA first fixes A and searches for ϕ. The value of ϕ is obtained when V_{in} is the smallest under the condition that A has a certain value. Then ϕ is fixed and the optimal value of A is searched. Similarly, the optimal value of A is obtained when V_{in} is the smallest for the condition when ϕ has a certain value.

The $step_A$ and U are the search step size of A and ϕ respectively. And a large step size will reduce algorithm's accuracy, while a small step size will lead to insufficient convergence speed. To balance convergence speed and algorithm accuracy, the convergence coefficients $[\alpha,\beta]$ are set to dynamically adjust $step_A$ and U. Through $[\alpha,\beta]$, the range of $[A,\phi]$ is gradually narrowed. Finally, the global optimum is obtained. The schematic diagram of ISA is shown in Fig. 8.

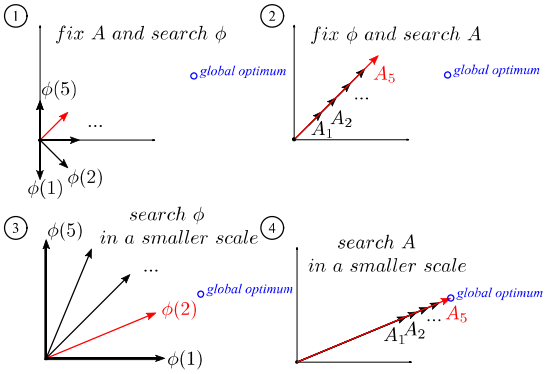

Fig. 8. Schematic diagram of ISA.

Fig. 9 demonstrates the flow chart of ISA, and the implementation of ISA is as follows:

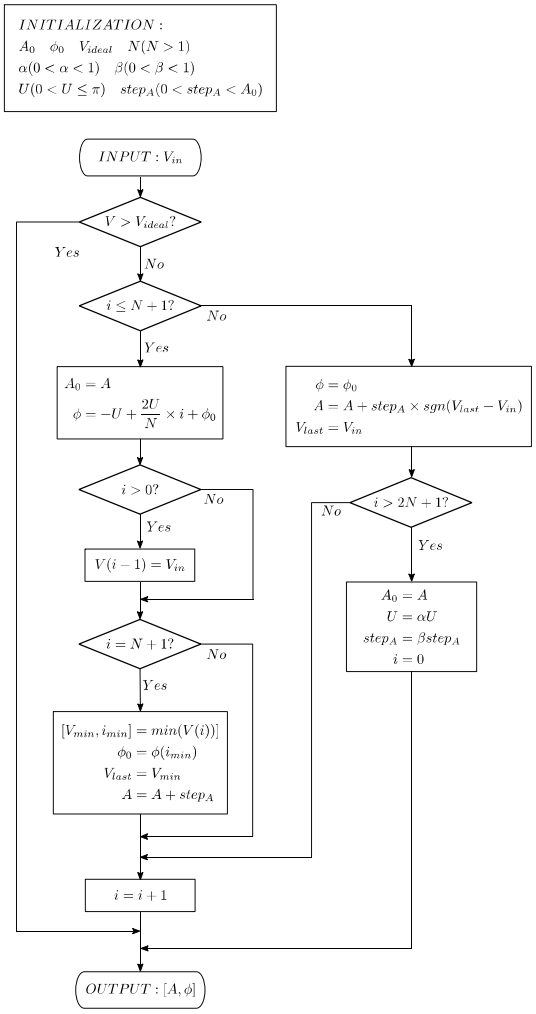

Fig. 9. Flow chart of ISA.

Initialization: define $[A_0,\phi_0,V_{\text{ideal}},N,U,step_A,\alpha,\beta]$. $[A_0,\phi_0]$ are the original value of $[A,\phi]$, N is the searching times of $[A,\phi]$, U is the searching limit of ϕ, $step_A$ is the searching step of A, and $[\alpha,\beta]$ are convergence coefficient of $[U,step_A]$.

Input: the mechanical time constant of the AMB system is greater than the electrical time constant of the AMB system. In order to avoid the influence of the AMB system mechanical transient process on measurement of V_{in} after changing $[A,\phi]$, V_{in} are calculated from the output of LMS adaptive filter Y every M_1 periods as follows:

$$V_{\text{in}}=\int_{(M_1-1)T}^{M_1T}Y^2(t)\mathrm{d}t \tag{19}$$

Comparing V_{in} and V_{ideal}, if $V_{\text{in}}\le V_{\text{ideal}}$, $[A,\phi]$ output is kept; otherwise, each time V_{in} is input, one of the following steps is executed to obtain a new $[A,\phi]$ output.

(In *Step* 0-*N*, (*N*+1) equally spaced ϕ located in $[-U+\phi_0,U+\phi_0]$ are sequentially output, and the corresponding V_{in} is obtained.)

Step 0: keep $A=A_0$ unchanged, then the new ϕ is obtained as:

$$\phi=\phi(1)=-U+\frac{2U}{N}\times 0+\phi_0 \tag{20}$$

Step i (0< i≤*N*): keep $A=A_0$ unchanged, and the new ϕ is obtained as:

$$\phi=\phi(i)=-U+\frac{2U}{N}\times i+\phi_0 \tag{21}$$

Then the vibration amplitude $V(i-1)$ is recorded corresponding to the last phase shifting angle $\phi(i-1)$:

$$V(i-1)=V_{\text{in}} \tag{22}$$

…

Step *N*+1: record $V(i-1)$ corresponding to $\phi(i-1)$, and search for the minimum value $V_{\min}$ of $V(i)$ (i = 0 to N) and its argument $i_{\min}$. Set ϕ_0 as follows:

$$\phi_0=-U+\frac{2U}{N}\times i_{\min}+\phi_0 \tag{23}$$

Then set $V_{\text{last}}=V_{\min}$, and keep $\phi=\phi_0$ unchanged. Define the searching direction of A as increase or decrease. Search A with $step_A$. Define the initial search direction as increase, then the iterative formula of A is:

$$A=A+step_A \tag{24}$$

…

Step i (*N*+2≤i≤2*N*+1): keep $\phi=\phi_0$ unchanged, and compare V_{last} and V_{in}. Search A based on the comparison results. The iterative formula of A is expressed as:

$$A=A+step_A\times\text{sgn}(V_{\text{last}}-V_{\text{in}}) \tag{25}$$

…

Step 2*N*+2: keep $\phi=\phi_0$ unchanged, and calculate A according to (25). At this point, a round of ISA is completed. In order to pursue higher accuracy, U and $step_A$ are reduced with the convergence coefficient $[\alpha,\beta]$ according to (26).

$$\begin{cases}U=\alpha U\\ step_A=\beta step_A\end{cases} \tag{26}$$

Set $A_0=A$, and return to *Step* 0 to start a new round of ISA.

The complete process of ISA is explained above. AFC is formed by adding the ISA to compensate the LMS adaptive filter, and the AFC's output $Y'(s)$ is expressed as:

$$Y'(s)=AY(s)e^{-s\frac{\phi}{\omega_n}} \tag{27}$$

The ω_n is the notch frequency of the AFC, which varies with the rotational speed. Y' is input into the PD controller, and a compensation current I_{comp} is generated. According to (2), I_{comp} produces a compensation force in AMB to restrain F_{dis}, then the vibration is suppressed.

If only fundamental vibration exists in the rotor, insert 1st order AFC into the AMB control system. In practice, there are harmonic vibrations caused by sensor runout other than the fundamental vibration caused by rotor unbalance. Therefore, the 1st-nth order AFCs are added to the AMB controller to suppress the fundamental and other harmonic vibrations. After that, the 1-DOF AMB control system diagram with the 1st-nth order AFCs is shown in Fig. 10.

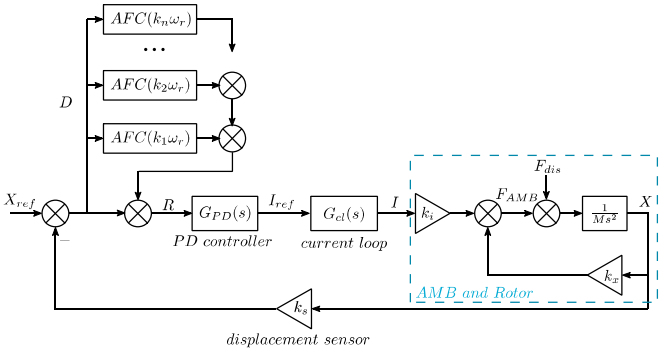

Fig. 10. 1-DOF AMB control system with 1st-nth order AFCs.

The decentralized control, which is discussed above, is applied in 5-DOFs AMB control system, and the 5-DOFs AMB can be controlled by five identical 1-DOF control systems with AFCs.

IV. Simulation Result

According to the mathematical model established in the previous sections, the simulation model of the 1-DOF AMB system with a rigid rotor is built in Simulink. The parameters

TABLE I
PARAMETERS OF AMB SYSTEM

Symbol	Parameter	Value
k_x	AMB force-displacement stiffness	961000 N/m
k_i	AMB force-current stiffness	72.06 N/A
M	Rotor mass	5.5 kg
K_P	Proportional coefficient of controller	40008
K_I	Integral coefficient of controller	100
K_D	Differential coefficient of controller	90.24
n	Rotational speed	5000 rpm
T_s	Sampling period	100 us

of the AMB system are shown in Table I.

In this section, the operation of the AMB system is simulated at the highest motor speed (5000 rpm). The frequencies of the disturbances are 1 and 3 times the rotational frequency in the simulation. The 1st and 3rd order AFCs based on ISA are applied to suppress them. The AFCs are launched at 2 s, and the ISA converges after about 10 s. The searching process of ISA is shown in Fig. 11, and the rotor displacement curve is shown is Fig. 12.

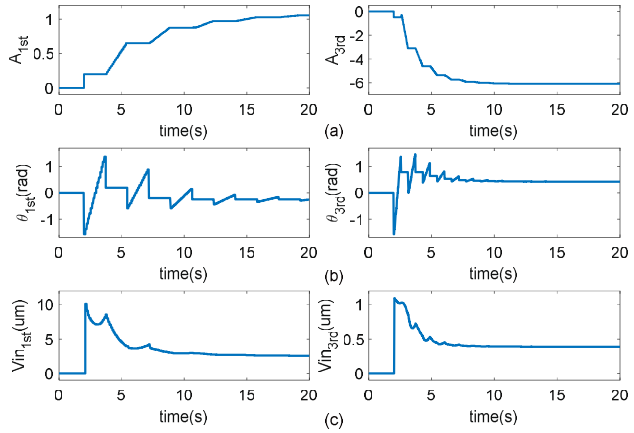

Fig. 11. Input and outputs in the searching process of 1st and 3rd order ISAs. (a) Output: A. (b) Output: ϕ (c) Input: V_{in}.

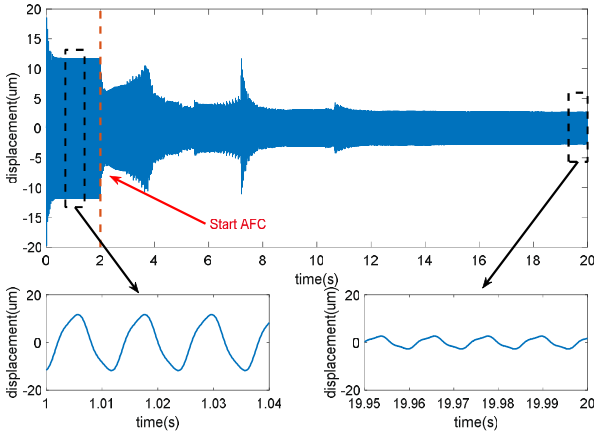

Fig. 12. Rotor displacement curve with and without AFC.

It can be concluded from Fig. 11 and Fig. 12 that after the ISA converges, the rotor vibration amplitude V_{in} is gradually reduced. V_{in} drops from 11.74 um to 2.70 um, decreasing by 77.0%. Performing FFT analysis to the rotor displacement, the 1st order vibration drops from 11.50 um to 2.54 um, decreasing by 77.9%. The 3rd order vibration drops from 1.09 um to 0.37 um, decreasing by 66.1%. Comparing the rotor displacement with and without AFCs, vibration performance is significantly improved by the AFCs.

It can be observed from Fig. 12 that during the search process, there are several significant spikes in the rotor displacement due to ISA. When ISA fixes A and searches for ϕ, $\phi(0)$ to $\phi(N)$ are applied to the AMB system in turns. When reaching $\phi(N)$, the ϕ_{best} with the minimum rotor vibration can be determined. Switching from $\phi(N)$ to ϕ_{best} causes an oscillation in the rotor displacement. However, this oscillation lasts only for a very short moment, and the rotor vibration during oscillation is smaller than that without ISA.

V. EXPERIMENTAL RESULT

To validate the effectiveness of the AFC based on the ISA, it is applied to a 5-DOFs AMB system with a rigid rotor. The setup of the AMB system and AMB controller for experimental validation is shown in Fig. 13. The position of TMB is indicated in Fig. 13, but the component is in the housing, thereby not visible. Its structure can be referred to Fig. 4. Primary parameters of the AMB system are given in Table I.

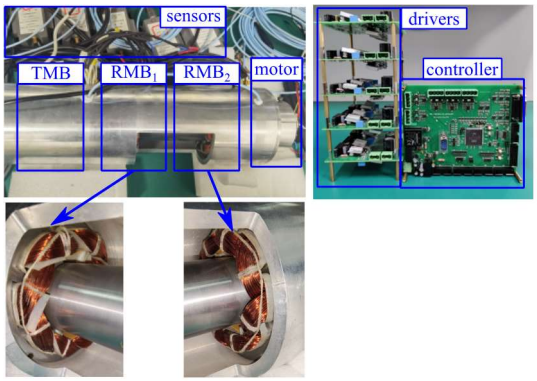

Fig. 13. Setup of 5-DOFs AMB system.

As 1st-3rd order vibrations are the main components of rotor vibration, the 1st-3rd order AFCs are applied in the controller. Experiments are carried out at the highest motor speed (5000 rpm) and entire speed range (1000-5000 rpm), respectively.

A. Vibration Suppression at a Fixed Speed

In the AMB used in this paper, there are primarily the 1st-3rd order vibrations in the radial 4-DOFs, and there is mainly 1st order vibration in the axial DOF. When rotational speed is 5000 rpm (83 Hz), vibration frequencies are 83 Hz, 167 Hz, and 250 Hz, respectively. To suppress these vibrations, AFCs with notch frequencies of 83 Hz, 167 Hz, and 250 Hz were added to the AMB control system for the radial 4-DOFs, and an AFC with a notch frequency of 83 Hz was added for the axial DOF.

To demonstrate the advantages of ISA proposed in this paper, AFCs based on ISA and FAC [25] are applied, and

vibration suppression effect of the ISA and FAC are compared. The transient processes of 5-DOFs AMB for the ISA and FAC are illustrated in Fig. 14. The 1st-3rd order components of rotor vibration were compared through FFT analysis, without any vibration suppression strategy, with FAC and with ISA. The spectral diagram of the 5-DOFs is shown in Fig. 15.

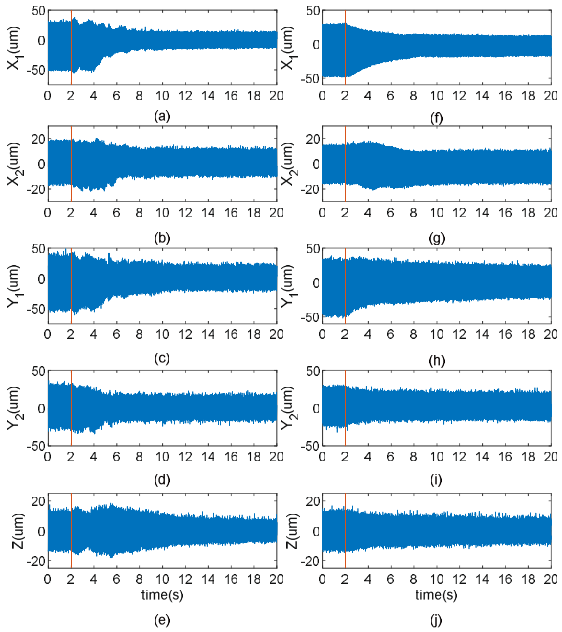

Fig. 14. 5-DOFs Rotor transient displacement tracks with different vibration suppression strategies (a-e) ISA (f-j) FAC.

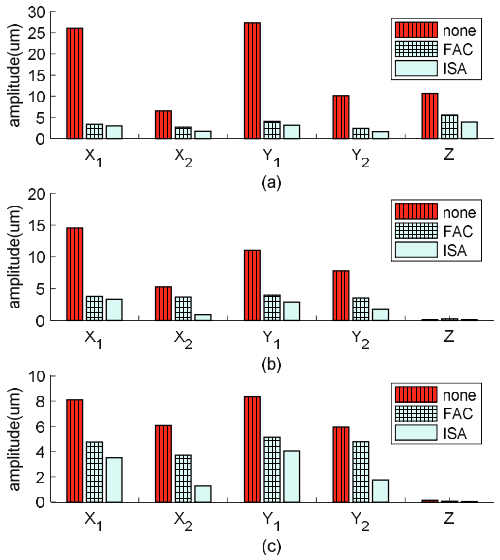

Fig. 15. Spectrums of the rotor vibration of 5-DOFs. (a) 1st order vibration. (b) 2nd order vibration. (c) 3rd order vibration.

The convergence speeds of ISA and FAC are fairly close when using the same search step size. The 1st-3rd order components of rotor vibration reduced by 83.36%, 76.84% and 62.94% respectively with AFCs based on ISA. When using the AFCs based on FAC, the 1st-3rd order components of rotor vibration reduced by 77.48%, 60.92% and 35.42%, respectively. Both ISA and FAC have effective vibration suppression for 1st order component of rotor vibration. However, ISA demonstrates superior suppression compared to FAC for 2nd-3rd order components of rotor vibration. The experiments show that ISA has a better vibration suppression for high order vibration.

B. Vibration Suppression over the Whole Speed Range

Over the whole speed range (1000-5000 rpm), the 1st-3rd order AFCs are applied to the radial 4-DOFs AMB control system, the 1st order AFC is applied to the axial DOF. The 1st-3rd order AFCs' notch frequencies are adaptive to the rotational speed ($\omega_{n1}=\omega_r, \omega_{n2}=2\omega_r, \omega_{n3}=3\omega_r$).

The vibrations in the X_1 and Y_1 DOFs are initially severe, and the suppression effect of ISA is quite remarkable. The rotor motions in these two DOFs are taken as an example.

The AFCs based on ISA are executed every 100 rpm, and the rotor displacement of the X_1 DOF is recorded before the AFCs start and after the AFCs converge. By performing FFT analysis on the rotor displacement, the vibration waterfall diagram of the rotor displacement is obtained in Fig. 16.

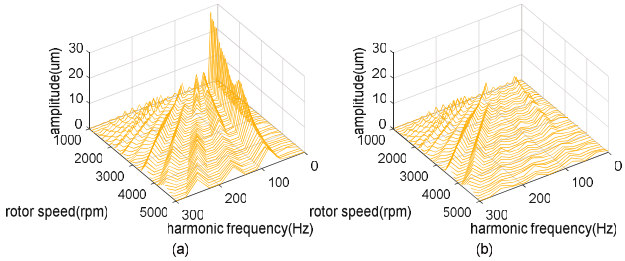

Fig. 16. Vibration waterfall of X_1 DOF in all speed range. (a) Without AFC. (b) With AFC.

It can be seen from Fig. 16 that over the whole speed range, there are mainly 1st-6th order vibrations in the AMB rotor. However, by the application of the 1st-3rd order AFCs, the vibration amplitude of the 1st-3rd order components decreases significantly.

The vibration amplitudes of 1st-6th order components with and without AFCs is presented in Fig. 17 to illustrate the changes in the 1st-6th order components of vibration more precisely. At 1000 rpm, with 1st-3rd order AFCs, the 1st-3rd order vibrations are decreased by 91.10%, 80.18%, and 83.81% respectively, and at 3000 rpm, the 1st-3rd order vibrations are decrease by 76.06%, 68.83%, and 54.79% respectively. The impact on 4th-6th order vibrations is insignificant.

The presented experimental results validate that the AFC proposed in this paper has an excellent vibration suppression effect over the full speed range of the motor. Moreover, the vibrations of the higher orders components do not deteriorate upon the addition of AFCs.

C. Vibration Suppression in the Variable Speed Range

It can be observed from Fig. 14 that the convergence time of ISA is approximately 10-20s. When operating in conditions with a variable speed range, the search space varies, potentially causing ISA to fail.

However, $[A,\phi]$, the outputs of ISA, establish the amplitude and phase relationship between rotor vibration and

the control current of the AMB. The $[A,\phi]$ obtained from the initial search can be utilized in subsequent processes.

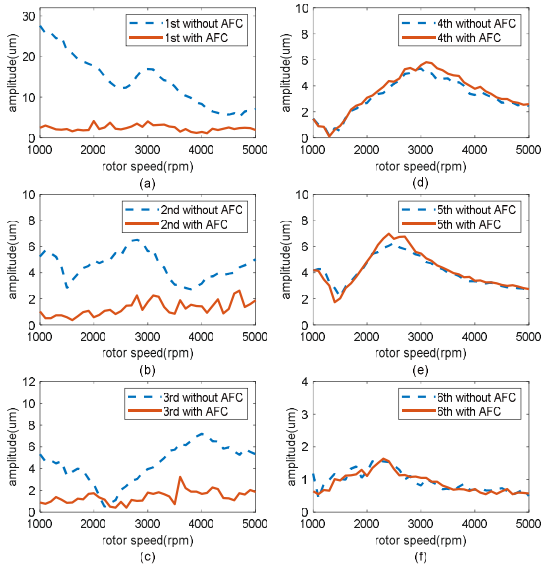

Fig. 17. 1st-6th order vibration amplitude of X_1 degree of freedom in all speed range. (a) 1st order vibration amplitude. (b) 2nd order vibration amplitude. (c) 3rd order vibration amplitude. (d) 4th order vibration amplitude. (e) 5th order vibration amplitude. (f) 6th order vibration amplitude.

To expand the application scope of ISA, it is recorded that $[A_k(\omega_r),\phi_k(\omega_r)]$ curves corresponding to different speed over the whole speed range experiments, as shown in Fig. 18, where k=1, 2, 3 represents vibration harmonic order, and ω_r denotes the rotational speed. Subsequently, $[A_k(\omega_r),\phi_k(\omega_r)]$ was directly integrated into the LMS adaptive filter. In conditions of variable speed, vibration suppression is achieved through the Look-Up Table (LUT) method.

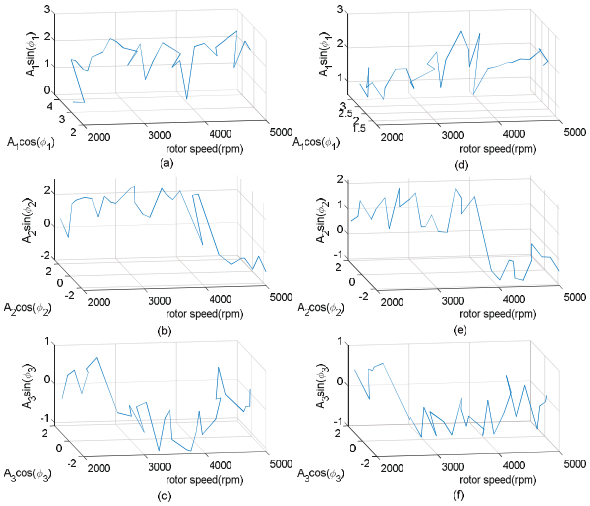

Fig. 18. $[A_k,\phi_k]$ tracks of the RMB_1 side obtained by ISA. (a-c) X_1 DOF (d-f). Y_1 DOF.

Based on $[A_k(\omega_r),\phi_k(\omega_r)]$, the adaptive filters with compensation (AFCs) using the LUT are constructed. At 5000 rpm, the AFCs were incorporated into the 5-DOFs AMB control system. The rotor vibration on the RMB_1 side (X_1 and Y_1 DOFs) is illustrated in Fig. 19. It's shown from Fig. 19 that the AFCs with LUT achieve convergence within 0.35 s, which shows an extremely short transient process compared with AFCs based on ISA. Moreover, the rotor vibration is the same as it was with the AFCs based on ISA. Possessing both convergence speed and suppression effectiveness, AFCs using LUT can be applied in variable speed condition.

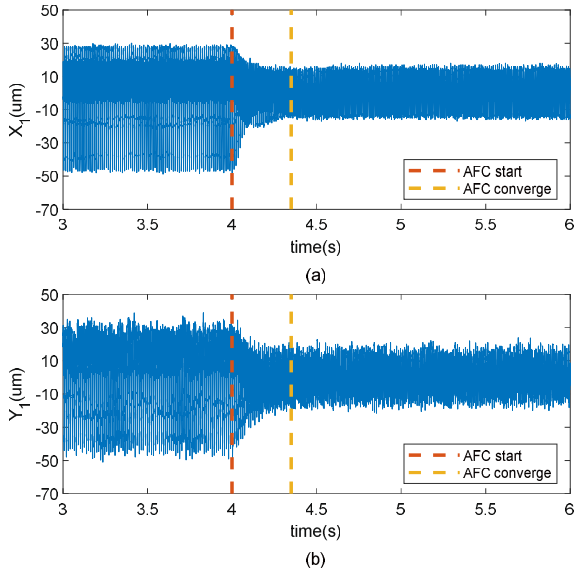

Fig. 19. Rotor vibration on the RMB_1 side (X_1 and Y_1 DOFs) using AFCs based on LUT. (a) X_1 DOF. (b) Y_1 DOF.

Within the variable speed range of 2000-5000 rpm, the AFCs with LUT were introduced into the 5-DOFs AMB control system, and the rotor orbits in RMB_1 side were recorded both with and without AFCs, as depicted in Fig. 20. It is concluded that within the variable speed condition, significant vibration suppression has been achieved.

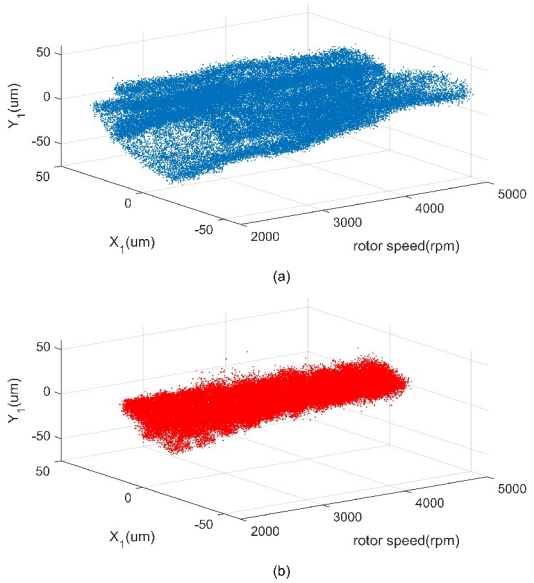

Fig. 20. Rotor orbits of RMB_1 side in variable speed range. (a) Without AFCs

based on LUT. (b) With AFCs based on LUT.

VI. CONCLUSION

Aiming at suppressing the rotor vibration in AMB, the first step involves detecting the vibration signals in the rotor displacement signals by the LMS adaptive filter. Subsequently, the proposed ISA is applied to compensate for $[A,\phi]$, the amplitude and phase of the output of the LMS adaptive filter. The Adaptive Filter with Compensation (AFC) is formed by combining the ISA and LMS adaptive filter, which help to generate a compensation force in AMB to suppress the rotor vibration effectively. As AFC does not require significant computational resources, AFCs with different frequencies can be connected in parallel to suppress vibrations with fundamental and other harmonic orders.

Comprehensive simulations and experiments were conducted on a 5-DOFs AMB system with a rigid rotor. There are 1st-3rd order vibrations in the rotor. Hence, the 1st-3rd order AFCs were added to the AMB controller.

Initially, at a fixed speed (5000 rpm), the vibration suppression effects of ISA and FAC were compared. Experimental results reveal that both ISA and FAC achieve great vibration suppression effects when dealing with the 1st order vibration. However, ISA exhibits superior vibration suppression effects on the 2nd and 3rd order vibrations.

Secondly, the ISA was executed every 100 rpm over the whole speed range (1000-5000 rpm) to verify its effects, and then the $[A,\phi]$ curve corresponding to speed is recorded.

Finally, based on the $[A,\phi]$ curve corresponding to rotational speed obtained in the previous step, the AFCs were constructed using the LUT, effectively suppressing rotor vibration in variable speed condition.

REFERENCES

[1] Chiba, Akira, *et al*, "Magnetic Bearings and Bearingless Drives," *Elsevier*, 2005.

[2] Bleuler, Hannes, and Matthew Cole, "Magnetic Bearings: Theory, Design, and Application to Rotating Machinery," Eds. Eric H. Maslen, and Gerhard Schweitzer. Berlin, Heidelberg: Springer-Verlag Berlin Heidelberg, 2009.

[3] Herzog R., Buhler P., Gahler C. *et al*, "Unbalance Compensation Using Generalized Notch Filters in the Multivariable Feedback of Magnetic Bearings," *IEEE Transactions on Control Systems Technology*, vol. 4, no, 5, pp. 580-586, 1996.

[4] Kejian. Jiang, Changsheng Zhu, and Ming Tang, "A Uniform Control Method for Imbalance Compensation and Automation Balancing in Active Magnetic Bearing-rotor Systems," *Journal of Dynamic Systems, Measurement, and Control*, vol. 134, no. 2, pp. 02100601-02100613, 2012.

[5] S. Zheng, B. Han, and R. Feng *et al*, "Vibration Suppression Control for AMB-supported Motor Driveline System Using Synchronous Rotating Frame Transformation," *IEEE Transactions on Industrial Electronics*, vol. 62, no. 9, pp. 5700-5708, 2015.

[6] C. Peng, S. Zheng, and Z. Huang *et al*, "Complete Synchronous Vibration Suppression for a Variable-speed Magnetically Suspended Flywheel Using Phase Lead Compensation," *IEEE Transactions on Industrial Electronics*, vol. 65, no. 7, pp. 5837-5846, July 2018.

[7] S. Zheng, Q. Chen and H. Ren, "Active Balancing Control of AMB-rotor Systems Using a Phase-shift Notch Filter Connected in Parallel Mode," *IEEE Transactions on Industrial Electronics*, vol. 63, no. 6, pp. 3777-3785, June 2016.

[8] Kai-Yew Lum, V. T. Coppola, and D. S. Bernstein, "Adaptive Autocentering Control for an Active Magnetic Bearing Supporting a Rotor with Unknown Mass Imbalance," *IEEE Transactions on Control Systems Technology*, vol. 4, no. 5, pp. 587-597, Sept. 1996.

[9] Chao Bi, Dezheng Wu, and Quan Jiang *et al*, "Automatic Learning Control for Unbalance Compensation in Active Magnetic Bearings," *IEEE Transactions on Magnetics*, vol. 41, no. 7, pp. 2270-2280, July 2005.

[10] Sung-Kyung Hong and R. Langari, "Robust Fuzzy Control of a Magnetic Bearing System Subject to Harmonic Disturbances," *IEEE Transactions on Control Systems Technology*, vol. 8, no. 2, pp. 366-371, March 2000.

[11] P. Cui, S. Li, and Q. Wang *et al*, "Harmonic Current Suppression of an AMB Rotor System at Variable Rotation Speed Based on Multiple Phase-shift Notch Filters," *IEEE Transactions on Industrial Electronics*, vol. 63, no. 11, pp. 6962-6969, Nov. 2016.

[12] C. Peng, J. He, and Z. Deng *et al*, "Parallel Mode Notch Filters for Vibration Control of Magnetically Suspended Flywheel in the Full Speed Range," *IET Electric Power Applications*, vol. 14, no. 9, pp. 1672-1678, 2020.

[13] H. Zhang, J. Liu, and R. Zhu *et al*, "Nonlinear Adaptive Harmonics Vibration Control for Active Magnetic Bearing System with Rotor Unbalance and Sensor Runout," *IEEE Sensors Journal*, vol. 21, no. 10, pp. 12245-12254, May15, 2021.

[14] J. He, Z. Deng, and C. Peng *et al*, "Reduction of the High-speed Magnetically Suspended Centrifugal Compressor Harmonic Vibration Using Cascaded Phase-shifted Notch Filters," *IEEE Sensors Journal*, vol. 21, no. 2, pp. 1315-1323, Jan. 15, 2021.

[15] Burrows, C. R., and M. N. Sahinkaya, "Vibration control of Multi-mode Rotor-bearing Systems," in *Proc. of the Royal Society of London. A. Mathematical and Physical Sciences*, vol. 386, no. 1790, pp. 77-94, 1983.

[16] Shi, Juan, Ron Zmood, and LiJiang Qin, "The Direct Method for Adaptive Feed-forward Vibration Control of Magnetic Bearing Systems." in *Proc. of 7th International Conference on Control, Automation, Robotics and Vision*, *2002. ICARCV 2002*, Singapore, 2002.

[17] Min Sig Kang, and Woo Hyun Yoon, "Acceleration Feedforward Control in Active Magnetic Bearing System Subject to Base Motion by Filtered-X LMS Algorithm," *IEEE Transactions on Control Systems Technology*, vol. 14, no. 1, pp. 134-140, Jan. 2006.

[18] C. Mao, and C. Zhu, "Vibration Control for Active Magnetic Bearing Rotor System of High-speed Flywheel Energy Storage System in a Wide Range of Speed," in *Proc. of 2016 IEEE Vehicle Power and Propulsion Conference (VPPC)*, Hangzhou, China, 2016, pp. 1-6.

[19] Kejian Jiang, and Zhu Changsheng. "Multi-frequency Periodic Vibration Suppressing in Active Magnetic Bearing-rotor Systems via Response Matching in Frequency Domain," *Mechanical Systems and Signal Processing*, vol. 25, no. 4, pp. 1417-1429, 2011.

[20] J. Shi, and H. Zhu, "Control Study for Compensating Rotor Vibration of Four-DOF Six-pole Hybrid Magnetic Bearings Based on Variable Step Size LMS Algorithm," *IEEE Journal of Emerging and Selected Topics in Power Electronics*, vol. 11, no. 2, pp. 1616-1626, April 2023.

[21] C. Peng, M. Zhu, and K. Wang *et al*, "A Two-Stage Synchronous Vibration Control for Magnetically Suspended Rotor System in the Full Speed Range," *IEEE Transactions on Industrial Electronics*, vol. 67, no. 1, pp. 480-489, Jan. 2020.

[22] Hongbo Sun, Dong Jiang, and Jichang Yang, "Synchronous Vibration Suppression of Magnetic Bearing Systems without Angular Sensors," *CES Transactions on Electrical Machines and Systems*, vol. 5, no. 1, pp. 70-77, 2021.

[23] L. Gong, and C. Zhu, "Vibration Suppression for Magnetically Levitated High-speed Motors Based on Polarity Switching Tracking Filter and Disturbance Observer," IEEE Transactions on Industrial Electronics, vol. 68, no. 6, pp. 4667-4678, June 2021.

[24] L. Gong, and C. Zhu, "Four-factor Polarity Switching Control for Synchronous Vibration Suppression of Active Magnetic Bearings Rigid Rotors System in the Full Rotational Speed Range," *IEEE Transactions on Industrial Electronics*, vol. 68, no. 12, pp. 11870-11880, Dec. 2021.

[25] J. Kejian, Z. Changsheng, and C. Liangliang, "Unbalance Compensation by Recursive Seeking Unbalance Mass Position in

Active Magnetic Bearing-rotor System," *IEEE Transactions on Industrial Electronics*, vol. 62, no. 9, pp. 5655-5664, Sept. 2015.

[26] L. Gong, and C. Zhu, "Synchronous Vibration Control for Magnetically Suspended Rotor System Using a Variable Angle Compensation Algorithm," *IEEE Transactions on Industrial Electronics*, vol. 68, no. 8, pp. 6547-6559, Aug. 2021.

[27] L. Gong, and C. S. Zhu, "Unbalance Compensation Method of an Active Magnetic Bearings-rigid Rotor System for High-speed Motors Based on Variable Angle Seeking Algorithm," *Proc. CSEE*, vol. 41, no. 19, pp. 6769-6778, 2021.

[28] J. H. Gao, D. Shi, and J. H. Ye *et al*, "The Relationship Between Pole Width and Load Capacity in Radial Magnetic Bearings," in *Proc. of 2023 IEEE 6th Student Conference on Electric Machines and Systems (SCEMS)*, HuZhou, China, 2023, pp. 1-6.

Jin-Hui Ye (S'21) was born in Guangxi, China, in 1999. He received the B.Eng. degree in electrical engineering in 2021 from Zhejiang University, Hangzhou, China, where he is currently working toward the M.S. degree in electrical engineering.

His research focuses on vibration suppression of active magnetic bearing.

Dan Shi was born in Luoyang, China, in 1986. She received the B.SC. and M.SC. degrees in Electrical Engineering at Zhejiang University Hangzhou, China, in 2009 and 2012 respectively, and the Ph.D. degree in Robotics Control and Intelligent Systems in École polytechnique fédérale de Lausanne (EPFL), Switzerland, in 2016. She is currently working as a postdoc in Department of Electrical Engineering in Zhejiang University. Her research interests include research and applications in high speed permanent magnet machines, design and control of magnetic bearings.

Yue-Sheng Qi (S'23) was born in Shandong, China, in 2001. He received the B.Eng. degree in electrical engineering in 2023 from Zhejiang University, Hangzhou, China, where he is currently working toward the M.S. degree in electrical engineering.

Jin-Hui Gao (S'21) was born in Zhejiang, China, in 1998. He received the B.Eng. degree in electrical engineering in 2021 from Zhejiang University, Hangzhou, China, where he is currently working toward the M.S. degree in electrical engineering.

His research focuses on optimized design of active magnetic bearing.

Jian-Xin Shen (M'98-SM'02) received the B.Eng. and M.Sc. degrees in electrical engineering from Xi'an Jiaotong University, Xi'an, China, in 1991 and 1994, respectively, and the Ph.D. degree in electrical engineering from Zhejiang University, Hangzhou, China, in 1997. He was with Nanyang Technological University, Singapore (1997-1999), The University of Sheffield, Sheffield, U.K. (1999-2002), and IMRA Europe SAS, U.K. Research Centre, Brighton, U.K. (2002-2004). Since 2004, he has been a Full Professor with Zhejiang University. He has authored more than 320 technical articles, and is the inventor of more than 40 patents. His main research interests include topologies, control and applications of permanent magnet machines and drives, and renewable energies. He received 12 paper awards from IEEE and international conferences, and was granted the Nagamori Award with recognition of his contribution to permanent magnet electrical machines and high-speed electrical machines. He is a Distinguished Lecturer of IEEE IAS and VTS societies, and was the General Chair of three IEEE sponsored international conferences. More information of him can be seen at https://person.zju.edu.cn/en/jxs.